Journal of Infrastructure Preservation and Resilience

RESEARCH Open Access

Probabilistic analysis of climate change impact on chloride-induced deterioration of reinforced concrete considering Nordic climate

Amro Nasr[1,2*], Dániel Honfi[3] and Oskar Larsson Ivanov[1]

Abstract

The impact of climate change on the deterioration of reinforced concrete elements have been frequently highlighted as worthy of investigation. This article addresses this important issue by presenting a time-variant reliability analysis to assess the effect of climate change on four limit states; the probabilities of corrosion initiation, crack initiation, severe cracking, and failure of a simply supported beam built in 2020 and exposed to chloride-induced corrosion. The historical and future climate conditions (as projected by three different emission scenarios) for different climate zones in Sweden are considered, including subarctic conditions where the impact of climate change may lead to large increases in temperature. The probabilities of all limit states are found to be: 1) higher for scenarios with higher GHG emissions and 2) higher for southern than for northern climate zones. However, the end-of-century impact of climate change on the probabilities of reaching the different limit states is found to be higher for northern than for southern climate zones. At 2100, the impact of climate change on the probability of failure can reach up to an increase of 123% for the northernmost zone. It is also noted that the end-of-century impact on the probability of failure is significantly higher (ranging from 3.5–4.9 times higher) than on the other limit states in all climate scenarios.

Keywords: Climate change, Infrastructure deterioration, Reinforcement corrosion, Monte Carlo simulation

Introduction

The climate system is undergoing considerable changes compared to the climate of the preindustrial era [1]. These changes can have substantial implications for the safety and performance of concrete structures with their service lives spanning over several decades. Recent studies have identified a large number of potential climate change impacts on infrastructure and the built environment [2–5] including accelerated deterioration of infrastructure and built environment elements [6–8], increased long-term deformations [2], increased wind-induced loads [8, 9], and increased intensity and/or frequency of flooding [10].

Among the identified risks, infrastructure and built environment deterioration is often highlighted as a major concern, even when climate change impacts are disregarded. Globally, the annual cost of corrosion is estimated to surpass 1.8 trillion USD [11, 12]. Country-specific estimates of the cost of corrosion (see [13] for Australia, [14] for the United States, and [15] for the United Kingdom) highlight the substantial economic consequences of deterioration. In Sweden, the maintenance costs of bridges and tunnels totalled ~ 1 billion SEK in 2019 (~ 0.1 billion USD) [16]. In addition to these exceptionally high economic consequences, the failure of infrastructure and built environment elements due to severe deterioration can lead to more dire consequences

*Correspondence: amro.nasr@kstr.lth.se

[1] Division of Structural Engineering, Lund University, Lund, Sweden
Full list of author information is available at the end of the article

related to risks to life and limb. The recent collapse of the Morandi Bridge over the Polcevera River, Genova, Italy in 2018 with 43 fatalities serves as an example of infrastructure failure that was, at least partly, attributed to deterioration [17, 18]. Another example is the recent collapse of the 12/13-story Champlain Towers South Condominium in Miami, Florida, the United States in 2021 with 98 fatalities [19, 20]. Although the exact causes of failure are still unclear, early investigations indicated extensive reinforcement corrosion as a likely cause among others. Hence, many recent studies highlight that assessing the impact of climate change on deterioration of the built environment is of paramount importance [6, 7, 11, 21, 22].

Noting that concrete is the most used construction material [23], studying the impact of climate change on the durability of concrete structural elements is especially attention-worthy. The current article addresses this important issue by probabilistically analyzing the impact of climate change on chloride-induced corrosion of reinforced concrete members in different climate zones, represented by four different Swedish counties; namely the southernmost county (Skåne), the northernmost county (Norrbotten), and two in-between counties (Uppsala and Gävleborg). For this purpose, a time-variant reliability analysis is presented to assess the effect of climate change on the probabilities of corrosion initiation, crack initiation, severe cracking, and failure of a simply supported beam exposed to chloride-induced corrosion. Furthermore, sensitivity analysis is conducted to compare the effect of climate change and changes in other parameters on the corrosion process. It should be mentioned that the validity of the used models for the various corrosion processes, like any model, has some limitations [24]. However, studying those limitations and improving the models is beyond the scope of the current paper. The main reason for choosing the selected models is their relative simplicity and the availability of previous studies that adopted them which facilitates the interpretation of the results in the current study. Although other deterioration mechanisms of reinforced concrete elements are possible (e.g., carbonation-induced corrosion [6, 25] and biodeterioration [26, 27]), chloride-induced corrosion is generally more damaging and more costly to repair [28]. Several recent studies have focused on probabilistically assessing the impact of climate change on chloride-induced corrosion [6, 7, 11, 25, 29–31]. However, none of these studies considered Nordic climate conditions with very different climate zones depending on the location. Furthermore, very few studies, if any, have explicitly considered all the limit states analyzed in the current study (i.e., corrosion initiation, crack initiation, severe cracking, and failure).

The article starts by briefly describing the different climate change scenarios and the projections of the environmental parameters involved in the analysis under these scenarios. The next section describes the chloride-induced corrosion modelling approach that is adopted in the study in detail. A section presenting an illustrative example of a simply supported beam that is exposed to chloride-induced corrosion is then introduced. Lastly, important discussion points and concluding remarks are highlighted.

Climate change scenarios and data

Several generations of climate change scenarios have been introduced in literature. In the study presented herein, the Representative Concentration Pathways (RCP) scenarios adopted in both the fifth and sixth assessment reports of the Intergovernmental Panel on Climate Change (IPCC) [1, 32] are considered. The RCP scenarios adopted are: 1) a low Greenhouse Gas (GHG) emissions scenario (referred to as RCP2.6) where strict regulations enforcing climate change mitigation would be implemented [33], 2) a high GHG emissions scenario (referred to as RCP8.5) that describes a highly energy-intensive future in the absence of climate change mitigation policies [34], and 3) a moderate emissions scenario (referred to as RCP4.5) that describes a future with GHG emission level that is between the other two scenarios [35]. It should be highlighted that under the current state of knowledge accurate probabilities cannot be reliably assigned to the different scenarios [36].

For producing the climate change data for the current study, the Rossby Centre regional Atmospheric climate model (RCA4) is adopted [37]. The RCA4 was operated over Europe at 50×50 km grid spacing. Aggregated data for the annual average relative humidity and temperature over each of the four studied counties is used. The climate change data used in the current study is based on RCA4 downscaling five different global climate models (GCMs) under RCP2.6, RCP 4.5, and RCP8.5. The different GCMs have been used in the context of CMIP5 (the fifth phase of the coupled model intercomparison project), see [38]. The five downscaled GCMs are: 1) EC-EARTH, 2) MIROC5, 3) HadGEM2-ES, 4) MPI-ESM-LR, and 5) NorESM1-M. These GCMs provided boundary conditions for producing the data used herein. Details about the five downscaled GCMs, respectively, can be found in [39–43]. A more elaborate description of the RCA4 climate projections can be found in [37]. The projections of the annual average relative humidity and temperature for the four considered counties are shown in Fig. 1. Large interannual variability is observed for both relative humidity and temperature projections. The interannual variability related to relative humidity is

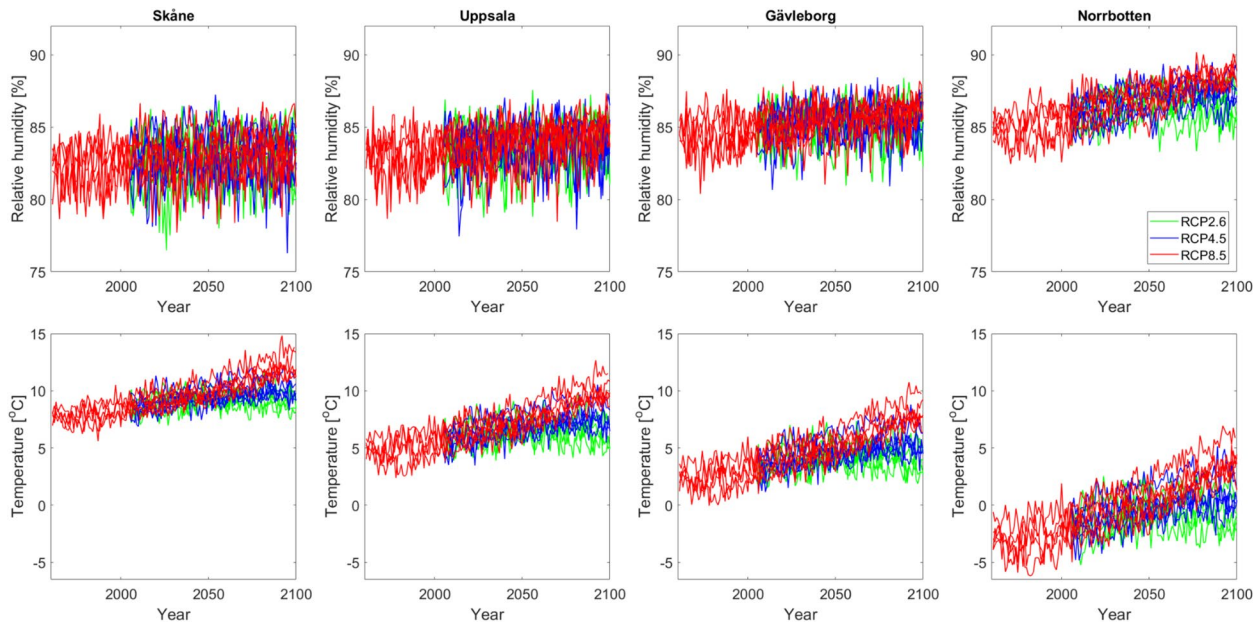

Fig. 1 Projections of the annual average values of relative humidity and temperature for Skåne, Uppsala, Gävleborg, and Norrbotten; counties are ordered from south (left) to north (right); multiple lines for each scenario represent different climate projections based on the five used GCMs (EC-EARTH, MIROC5, HadGEM2-ES, MPI-ESM-LR, and NorESM1-M)

smaller for northern (i.e., Norrbotten) than for southern counties (i.e., Skåne). It can generally be noted that Norrbotten has the highest while Skåne has the lowest relative humidity. On the other hand, Skåne has the highest while Norrbotten has the lowest temperature. For relative humidity, there is virtually no clear trend in all counties except Norrbotten where an increasing trend over time is observed. For temperature, on the other hand, a clear warming trend is observed for all counties (particularly in the highest emissions scenario, i.e., RCP8.5). For Monte Carlo simulation in Sect. 4, the annual average relative humidity and temperature data for each RCP scenario were fitted to a normal distribution.

Modelling chloride-induced corrosion

Reinforcement steel in sound concrete is surrounded by a passive oxide film. This passive layer is formed due to the high alkalinity of the concrete pore solution [44, 45]. Exposure to chlorides (from, e.g., sea salt spray, seawater wetting, and/or deicing salts), however, can lead to the breakdown of this protective layer and subsequently corrosion of reinforcement steel. The corrosion process is described by two phases [6, 25, 29, 45]: 1) the corrosion initiation phase and 2) the corrosion propagation phase. The time it takes for chlorides to penetrate to the level of the reinforcement and accumulate in sufficient quantities to break down the protective film and initiate the corrosion process (i.e., reach a critical chloride concentration) is known as the corrosion initiation time. Following corrosion initiation, the corrosion propagation phase starts. This phase is governed by the reinforcement corrosion rate (i.e., corrosion current density). The formation of rust due to corrosion propagation (which can have a volume that is twice to six times that of the corroded steel [46]) results in internal stresses which lead to cover cracking and eventually spalling of the concrete surrounding the reinforcement. The remainder of this section outlines the models used in this article to describe the corrosion process.

Time to corrosion initiation

Several models can be found in literature for estimating the corrosion initiation time [47–49]. One of the most widely used models is the model proposed in [48] based on Fick's second law of diffusion [6, 25, 29, 50, 51]. Based on this model the corrosion initiation time (t_i) [*years*] is calculated as follows:

$$t_i = \delta_{t_i} \cdot \left[\frac{x^2}{4 \cdot k_e \cdot k_c \cdot k_t \cdot D_c(T, RH) \cdot t_0^{n_{cl}}} \cdot \left[erf^{-1}\left(1 - \frac{C_{cr}}{C_s}\right)\right]^{-2} \right]^{\frac{1}{1-n_{cl}}} \quad (1)$$

where δ_{t_i} is a model uncertainty factor to account for the idealization implied by Fick's second law, x is the concrete cover depth [mm], k_e, k_c, and k_t are environment, curing, and test method factors respectively, $D_c(T, RH)$ is the chloride diffusion coefficient as a function of temperature

(T) and relative humidity (RH), t_0 is the reference time [$years$], n_{cl} is age factor, erf^{-1} represents the inverse of the Gaussian error function, and C_{cr} and C_s are the critical chloride concentration and the chloride concentration at the reinforcement surface, respectively. In Eq. (1), the dependency of $D_c(T, RH)$ on T and RH is evaluated as follows [25]:

$$D_c(T, RH) = D_{c,ref} \cdot F_1(T) \cdot F_2(RH) \tag{2}$$

with

$$F_1(T) = e^{\frac{U_c}{R} \cdot \left(\frac{1}{T_{ref}} - \frac{1}{273+T} \right)} \tag{3}$$

$$F_2(RH) = e^{\left(1 + \frac{(1-RH)^4}{(1-RH_c)^4} \right)^{-1}} \tag{4}$$

where $D_{c,ref}$ is the reference diffusion coefficient at a reference temperature of 20 °C (i.e.,$T_{ref} = 293K$) and a reference relative humidity of 75% (i.e.,$RH_c = 0.75$), U_c and R are the activation energy of chloride diffusion process ($4 \times 10^4 \frac{J}{mol}$) and the gas constant ($8.314 \frac{J}{mol \cdot K}$) respectively, and T and RH are the temperature [°C] and the relative humidity in decimals (e.g., 0.8 for 80% relative humidity), respectively.

Corrosion rate

Similar to the corrosion initiation time, several models for predicting the corrosion rate can be found in literature, see [24] for a comparison between a number of different models. For the purpose of the current article, the model proposed by [52] is used along with the temperature, relative humidity, and chloride concentration modification factors proposed by [53], see also [25, 29]:

$$i_{corr}(t) = \delta_{i_{corr}} \cdot \left[\frac{37.8 \cdot (1 - \frac{w}{c})^{-1.64}}{x} \cdot 0.85 \cdot (t - t_i)^{-0.29} \cdot f_T \cdot f_{RH} \cdot f_{Cl} \right] \tag{5}$$

where $i_{corr}(t)$ is the corrosion current density [$\frac{\mu A}{cm^2}$], $\delta_{i_{corr}}$ is a model uncertainty factor (represented by a Weibull distribution with a mean of 1.355 and a coefficient of variation (COV) of ~ 0.57 [24]), $\frac{w}{c}$ is the water to cement ratio, t is the concrete age [$years$], f_T is a modification factor accounting for a temperature deviation from the 20 °C reference temperature considered in [52], f_{RH} is a modification factor accounting for a relative humidity deviation from the 75% reference relative humidity considered in [52], and f_{Cl} is a modification factor accounting for the increase in chloride concentration during the propagation phase. The different modification factors are evaluated as follows [25, 29]:

$$f_T = (1 + K_T \, [T - 20]) \tag{6}$$

with

$$K_T = \begin{cases} 0.025 \ if \ T \leq 20°C \\ 0.073 \ if \ T > 20°C \end{cases} \tag{7}$$

and

$$f_{RH} = e^{-6000 \left(\frac{RH - 0.75}{1} \right)^6} \tag{8}$$

$$f_{Cl} = \frac{C_s + C_{cr}}{2 \cdot C_{cr}} \tag{9}$$

It is worth highlighting that varying values for the model uncertainty factor ($\delta_{i_{corr}}$) can be found in literature [24, 25, 52]. The value adopted in the current study is based on recent findings in [24]. In Lu et al. [24], the authors compared the predictions of the corrosion rate model adopted herein, as well as seven other models, to experimental results and found that the model uncertainty factor ($\delta_{i_{corr}}$) is best described by a Weibull distribution with a mean of 1.355 and a COV of ~ 0.57. However, Vu and Stewart [52] assumed a uniform distribution with a mean of 1.0 and a COV of 0.2 for this factor. It should be noted that, the different estimates of this factor do not take into account the three aforementioned modification factors (i.e., f_T, f_{RH}, and f_{Cl}) which would be expected to improve the model predictions (i.e., reduce the uncertainty). Deriving more reliable estimates of this uncertainty factor should be addressed in future studies.

Time to initiation of cover cracking

Similar to both the corrosion initiation time and the corrosion rate, various models exist for the prediction of corrosion-induced cover cracking [54]. In the current article, the model developed by [55] and later recommended in DuraCrete [48] is adopted. The time to corrosion-induced cover cracking is predicted as follows [54]:

$$x_{cr} = 83.8 + 7.4 \cdot \frac{x}{d_{r,0}} - 22.6 \cdot f_{ct} \tag{10}$$

$$t_{cr} = \frac{x_{cr}}{11.6 \cdot i_{corr}} + t_i \tag{11}$$

where $d_{r,0}$ is the initial reinforcement bar diameter [mm], f_{ct} is the splitting tensile strength of concrete [MPa], x_{cr} is the critical corrosion penetration at which cover cracking occurs [μm], and t_{cr} is the age at which cover cracking initiates [$years$].

Time to severe cracking (i.e., spalling)

Similar to the time to corrosion initiation, corrosion rate, and the time to crack initiation, several models that describe crack propagation can be found in literature

[56, 57]. In the current article, the model developed by [57] is adopted. The age when a limit crack width $w_{lim}[mm]$ is reached can be evaluated as follows:

$$t_{sp} = k_R \cdot \frac{w_{lim} - 0.05}{k_{Conf.} \cdot \delta_{r_{crack}} \cdot r_{crack}} \cdot \frac{0.0114}{i_{corr-20}} + t_{cr} \quad (12)$$

where t_{sp} is the age of severe cracking (i.e., the time when w_{lim} is reached, also referred to as concrete spalling) [*years*], $k_{Conf.}$ is the confinement factor that represents the effect of confinement on crack propagation (taken as 1.0 [6]), $\delta_{r_{crack}}$ represents the model uncertainty factor for the rate of crack propagation model (represented by a normal distribution with a mean of 1.04 and a COV of 0.09 [6]), $i_{corr-20}$ is the corrosion current density $[\frac{\mu A}{cm^2}]$ at 20 °C (represented by a lognormal distribution with a mean of 2.586 and COV of 0.67 for elements under cyclic wetting and drying [6, 48]), k_R is the rate of loading correction factor, and r_{crack} is the rate of crack propagation $[\frac{mm}{hr}]$. In the current article, similar to in [6], severe cracking is represented by a limit crack width of 1 mm. k_R and r_{crack} are evaluated using Eqs. (13), (14) and (15), respectively [6]:

$$k_R \approx 0.95 \cdot \left[e^{-\frac{0.3 \cdot i_{corr(exp)}}{i_{corr-20}}} - \frac{i_{corr(exp)}}{2500 \cdot i_{corr-20}} + 0.3 \right] \quad (13)$$

$$r_{crack} = 0.0008 \cdot e^{-1.7 \psi_{cp}} \quad (14)$$

with

$$\psi_{cp} = \frac{x}{d_{r,0} \cdot f_t} \quad (15)$$

where $i_{corr(exp)}$ is the accelerated corrosion rate used to derive r_{crack} (100 $\frac{\mu A}{cm^2}$ [6]), ψ_{cp} is a cover cracking parameter, and f_t is the direct tensile strength of concrete [*MPa*].

Loss of reinforcing steel area

Chloride-induced corrosion of reinforcement in concrete structures can be divided into two types: 1) uniform corrosion and 2) pitting corrosion [44, 45, 58], see Fig. 2. Uniform corrosion (also referred to as general corrosion), as the name implies, results in a uniform loss of metal over the perimeter of a reinforcing bar. On the other hand, pitting corrosion is non-uniform over the perimeter of a reinforcing bar and results in a more localized loss of metal. In this subsection, the models used to assess the loss of reinforcing steel area due to both types of corrosion are outlined.

Uniform corrosion

The time-dependent cross-sectional area of one steel reinforcement bar due to uniform corrosion ($A_{st,U}(t)$) can be evaluated as follows [47]:

$$A_{st,U}(t) = \begin{cases} d_{r,0}^2 \cdot \frac{\pi}{4} & if\ t \le t_i \\ d_r(t)^2 \cdot \frac{\pi}{4} & if\ t_i < t < t_i + \frac{d_{r,0}}{r_{corr}} \\ 0 & if\ t \ge t_i + \frac{d_{r,0}}{r_{corr}} \end{cases} \quad (16)$$

where $d_{r,0}$ is the initial reinforcement bar diameter before corrosion [*mm*], $d_r(t)$ is the reinforcement bar diameter at age t [*mm*], and r_{corr} is the annual metal loss per unit surface area $[\frac{mm}{year}]$. $d_r(t)$ and r_{corr} are evaluated as in Eqs. (17) and (18), respectively, based on i_{corr} $[\frac{\mu A}{cm^2}]$ [25, 47]:

$$d_r(t) = d_{r,0} - 0.0232 \cdot \int_{t_i}^{t} i_{corr}(t) dt \quad (17)$$

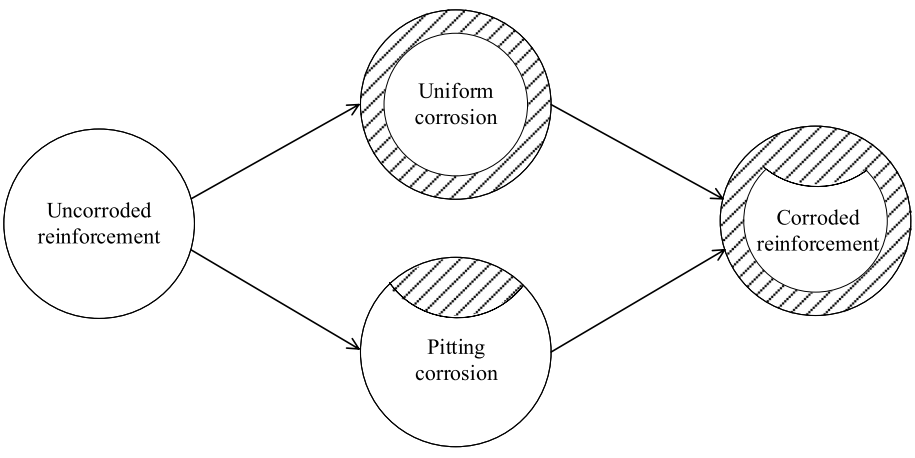

Fig. 2 Uniform and pitting corrosion, hatching indicates corroded steel

$$r_{corr} = 0.0116 \cdot i_{corr} \tag{18}$$

Pitting corrosion

One of the most frequently used models for estimating the loss of reinforcement bar cross-sectional area due to pitting corrosion is the hemispherical model developed by Val and Melchers [59]. Based on this model, the residual cross-sectional area of one reinforcing steel bar after the formation of a deep pit ($A_{st,DP}(t)$) can be calculated as follows:

$$A_{st,DP}(t) = \begin{cases} A_{st,0} - A_1 - A_2 & if\ p(t) \le \frac{d_{r,0}}{\sqrt{2}} \\ A_1 - A_2 & if\ \frac{d_{r,0}}{\sqrt{2}} < p(t) \le d_{r,0} \\ 0 & p(t) > d_{r,0} \end{cases} \tag{19}$$

with

$$A_1 = \frac{1}{2} \cdot \left(\theta_1 \cdot \left(\frac{d_{r,0}}{2} \right)^2 - a \cdot \left| \frac{d_{r,0}}{2} - \frac{p(t)^2}{d_{r,0}} \right| \right) \tag{20}$$

$$A_2 = \frac{1}{2} \cdot \left(\theta_2 \cdot p(t)^2 - a \cdot \frac{p(t)^2}{d_{r,0}} \right) \tag{21}$$

$$\theta_1 = 2 \cdot arcsin\left(\frac{a}{d_{r,0}} \right) \tag{22}$$

$$\theta_2 = 2 \cdot arcsin\left(\frac{a}{2 \cdot p(t)} \right) \tag{23}$$

$$a = 2 \cdot p(t) \cdot \sqrt{1 - \left(\frac{p(t)}{d_{r,0}} \right)^2} \tag{24}$$

$$p(t) = 0.0116 \cdot i_{corr} \cdot (t - t_i) \cdot R \tag{25}$$

where $A_{st,0}$ is the original reinforcement area before corrosion [mm^2], $p(t)$ is the pitting penetration at time t [mm], a is the width of a deep pit [mm], and R is the ratio between the maximum penetration of pitting to the average penetration of uniform corrosion. Varying values of R can be found in literature [44]. For instance, according to [60] this ratio can be modelled as following a Gumbel distribution with parameters depending on the bar surface area and length. On the other hand, in [61] this ratio is assumed as uniformly distributed between 4.0 and 6.0. The latter distribution is adopted in the current article. Following the evaluation of $A_{st,U}(t)$ and $A_{st,DP}(t)$, the residual cross-sectional area of one reinforcing steel bar at a pit location due to both uniform and pitting corrosion ($A_{st,U+P}$) [mm^2] can be computed as follows [25, 58]:

$$A_{st,U+P} = \left(A_{st,U}(t) - A_{st,0} \right) \cdot \left(1 - \frac{a}{2 \cdot d_{r,0}} \right) + A_{st,DP}(t) \tag{26}$$

Effect of corrosion on steel strength

In addition to the reduction of reinforcement cross-sectional area, corrosion also affects the mechanical properties [62] and ductility [63] of reinforcement steel. Both the ductility and strength of reinforcement steel are reduced by corrosion (see also [64]). However, this reduction is relatively small compared to the reduction in the cross-sectional area (see Sect. 3.5) [62]. In the current article, the effect of corrosion on the reinforcement yield strength is considered as follows [62, 65]:

$$f_y(t) = \left(1 - \delta_{Q_{cr}} \cdot Q_{cr} \right) \cdot f_{y,0} \tag{27}$$

with

$$Q_{cr} = \frac{A_{st,0} - A_{st,U+P}(t)}{A_{st,0}} \tag{28}$$

where $\delta_{Q_{cr}}$ is a model uncertainty factor, $f_{y,0}$ is the initial yield strength before corrosion and $f_y(t)$ is the yield strength at age t. Although it is acknowledged that reinforcement corrosion has several other effects (e.g., reduction of concrete strength, reduction of steel–concrete bond strength, reduction of low cycle fatigue and buckling strength [29, 64]), these effects are not considered in the current article.

Effect of climate change on the deterioration of a simply supported beam and its long-term flexural reliability

As shown by the models in the previous section, changes to the annual average relative humidity and temperature due to climate change affect the corrosion process by altering the corrosion initiation time (due to changing the diffusion coefficient) and the corrosion rate which subsequently affect the other models presented. In this section the effect of climate change on chloride-induced corrosion of a simply supported beam exposed to marine environment and its long-term reliability are analyzed using Monte Carlo simulation. For this purpose, three different climate change scenarios (i.e., RCP2.6, RCP4.5, and RCP8.5) as well as the historical climate (1961–1990) are considered for four different Swedish counties (see Fig. 3.); namely the southernmost county (Skåne), the northernmost county (Norrbotten), and two in-between counties (Uppsala and Gävleborg). The considered example is adapted from Val [44] and is shown in Fig. 4. It is assumed that the beam is built in 2020 and was cured for 28 days. Additionally,

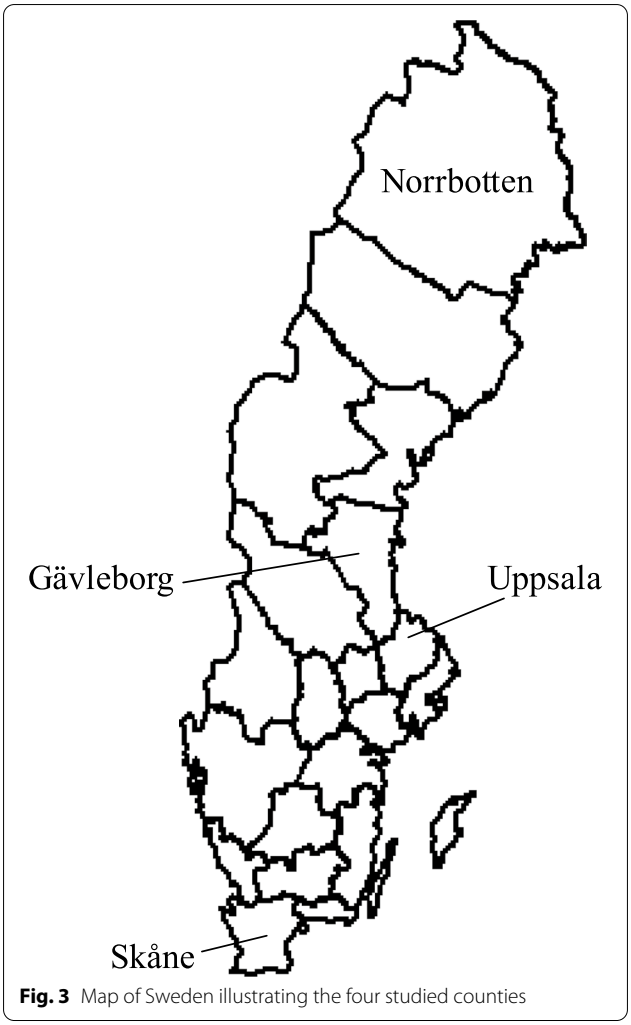

Fig. 3 Map of Sweden illustrating the four studied counties

the beam is assumed to be under atmospheric exposure conditions and to be exposed to many humid-dry cycles. The beam is subjected to uniformly distributed dead and live (sustained and extraordinary) loads. As in [44], the ratio of the nominal values of the live (Q_n) and dead (G_n) loads is assumed as $\frac{Q_n}{G_n} = 1.75$ with $Q_n = 35\frac{kN}{m}$ and $G_n = 20\frac{kN}{m}$. The beam has a length of 10 m, a height of 0.8 m, a width of 0.35 m and is reinforced with nine No. 8 bars. This example is suitable for the purpose of the current article as it does not involve the assessment of climate change impacts on environmental loads (e.g., snow, temperature, or wind loads) which is out of the scope of the current article. However, it should be highlighted that the considered example is only illustrative, and the same procedure adopted herein can be generally applied to other cases.

As in previous studies, e.g., [65], the maximum bending moment at mid span is considered for assessing the flexural reliability of the beam. Although failure can occur at other sections along the beam due to pitting corrosion [44], this is not considered herein. The following limit state function is considered [65]:

$$g(t) = \delta_{M_R} \cdot n \cdot A_{st,U+P}(t) \cdot f_y(t) \cdot \left(d - K_{M_R} \cdot \frac{n \cdot A_{st,U+P}(t) \cdot f_y(t)}{b \cdot f_c} \right) - M_S \tag{29}$$

with

$$M_S = \frac{(G + Q_S + Q_E) \cdot L^2}{8} \tag{30}$$

where δ_{M_R} is the flexural resistance model uncertainty factor, d is the effective depth of the cross section $[mm]$, K_{M_R} represents the flexural resistance ratio, b is the section width $[mm]$, f_c is the compressive strength of concrete $[MPa]$, M_S is the applied bending moment at midspan $[N \cdot mm]$, G is the dead load $\left[\frac{kN}{m}\right]$, Q_s is the sustained live load $\left[\frac{kN}{m}\right]$, Q_E is the extraordinary live load $\left[\frac{kN}{m}\right]$, and L is the beam length $[mm]$. Failure is defined as the event that $g(t)$ becomes less than or equal to zero (i.e., the beam flexural resistance is lower than or equal to the applied bending moment):

$$P_f(t) = P(g(t) \leq 0) \tag{31}$$

where $P_f(t)$ is the probability of failure at time t. The variables considered in this illustrative example are shown in Table 1.

Probability of corrosion initiation, crack initiation, and severe cracking

Figures 5, 6 and 7 show the probabilities of corrosion initiation, crack initiation and severe cracking (i.e., spalling),

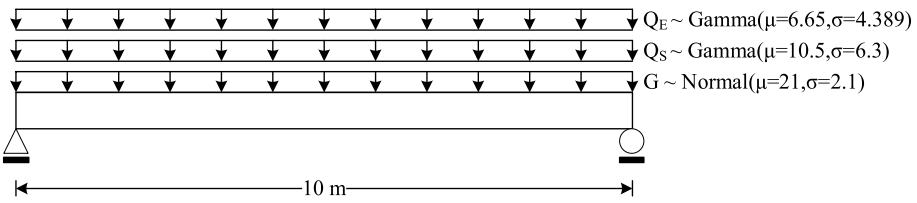

Fig. 4 The studied simply supported beam

Table 1 Variables considered in the illustrative example

Variable	Unit	Distribution	Mean	Standard deviation	Equation(s)	Reference
x	$[mm]$	Normal	50.0	6.0	(1, 5, 10, 15)	[65]
δ_{t_i}	$[-]$	Lognormal	1.0	0.05	(1)	[51]
k_e	$[-]$	Gamma	0.676	0.114	(1)	[51]
k_c	$[-]$	Beta	0.8	0.1	(1)	[51]
k_t	$[-]$	Normal	0.832	0.024	(1)	[51]
t_0	$[days]$	Deterministic	28	-	(1)	[51]
n_{cl}	$[-]$	Beta	0.362	0.245	(1)	[51]
C_{cr}	$[\%wtbr]$	Normal	0.9	0.15	(1, 9)	[51]
A_{cs}[a]	$[\%wtbr]$	Normal	2.565	0.356	-	[51]
ε_{cs}[a]	$[\%wtbr]$	Normal	0	0.405	-	[51]
$D_{c,ref}$	$[\frac{mm^2}{year}]$	Normal	473	47.3	(2)	[64]
$\delta_{i_{corr}}$	$[-]$	Weibull	1.355	0.775	(5)	[24]
$\frac{w}{c}$	$[-]$	Lognormal	0.5	0.05	(5)	[51, 66]
$d_{r,0}$	$[mm]$	Normal	25.4	1.016	(10, 15–17, 19–22, 24, 26)	[44, 64]
f_{ct}	$[MPa]$	Normal	$0.69\sqrt{E(f_c)}$[c]	$0.138\sqrt{E(f_c)}$[c]	(10)	[52]
$i_{corr-20}$	$[\frac{\mu A}{cm^2}]$	Lognormal	2.586	1.733	(12, 13)	[6]
$i_{corr(exp)}$	$[\frac{\mu A}{cm^2}]$	Deterministic	100	-	(13)	[6]
$\delta_{r_{crack}}$	$[-]$	Normal	1.04	0.0936	(12)	[6]
f_t	$[MPa]$	Normal	$0.53\sqrt{E(f_c)}$[c]	$0.069\sqrt{E(f_c)}$[c]	(15)	[6]
R[b]	$[-]$	Uniform	5.0	~0.577	(25)	[61]
$f_{y,0}$	$[MPa]$	Lognormal	490	49	(27)	[44]
$\delta_{Q_{cr}}$	$[-]$	Lognormal	0.005	0.0006	(27)	[65]
δ_{M_R}	$[-]$	Normal	1.0	0.1	(29)	[65]
n	$[-]$	Deterministic	9	-	(29)	[44]
K_{M_R}	$[-]$	Normal	0.6	0.03	(29)	[65]
d	$[mm]$	Normal	710	14.2	(29)	[44]
b	$[mm]$	Normal	350	7	(29)	[44]
f_c	$[MPa]$	Lognormal	26.2	4.716	(29)	[44]
G	$[\frac{kN}{m}]$	Normal	21	2.1	(30)	[44]
Q_S	$[\frac{kN}{m}]$	Gamma	10.5	6.3	(30)	[44]
Q_E	$[\frac{kN}{m}]$	Gamma	6.65	4.389	(30)	[44]
L	$[mm]$	Deterministic	10,000	-	(30)	[44]

% wt br percent weight of binder

[a] A_{cs} *and* ε_{cs} are parameters used to calculate C_s as follows: $C_s = A_{cs} \cdot E\left(\frac{w}{c}\right) + \varepsilon_{cs}$ with $E(\cdot)$ representing the expected value

[b] R is represented by a uniform distribution with a lower limit of 4.0 and an upper limit of 6.0 [61]

[c] $E(\cdot)$ represents the expected value

respectively, under historical (1961–1990) and future climate conditions for the four studied counties. It can be seen that the probability of corrosion initiation is higher for scenarios with higher GHG emissions. This is mainly due to the higher annual average temperatures in these scenarios. Although the increasing trend of the relative humidity in Norrbotten (see Fig. 1) can also have a negative effect on corrosion initiation (i.e., can accelerate corrosion initiation), the negative effect of the increasing trend of the temperature is significantly higher. For all climate scenarios, the probability of corrosion initiation is highest for Skåne followed by Uppsala, Gävleborg, and Norrbotten, respectively (i.e., decreasing trend from south to north).

The probabilities of crack initiation and severe cracking show trends similar to the probability of corrosion initiation; i.e., 1) The probabilities are higher for RCP8.5 followed by RCP4.5, RCP2.6, and the historical climate, respectively, and 2) the probabilities are higher for Skåne, followed by Uppsala, Gävleborg, and Norrbotten, respectively. While the end-of-century probability of crack initiation is approximately identical to the probability

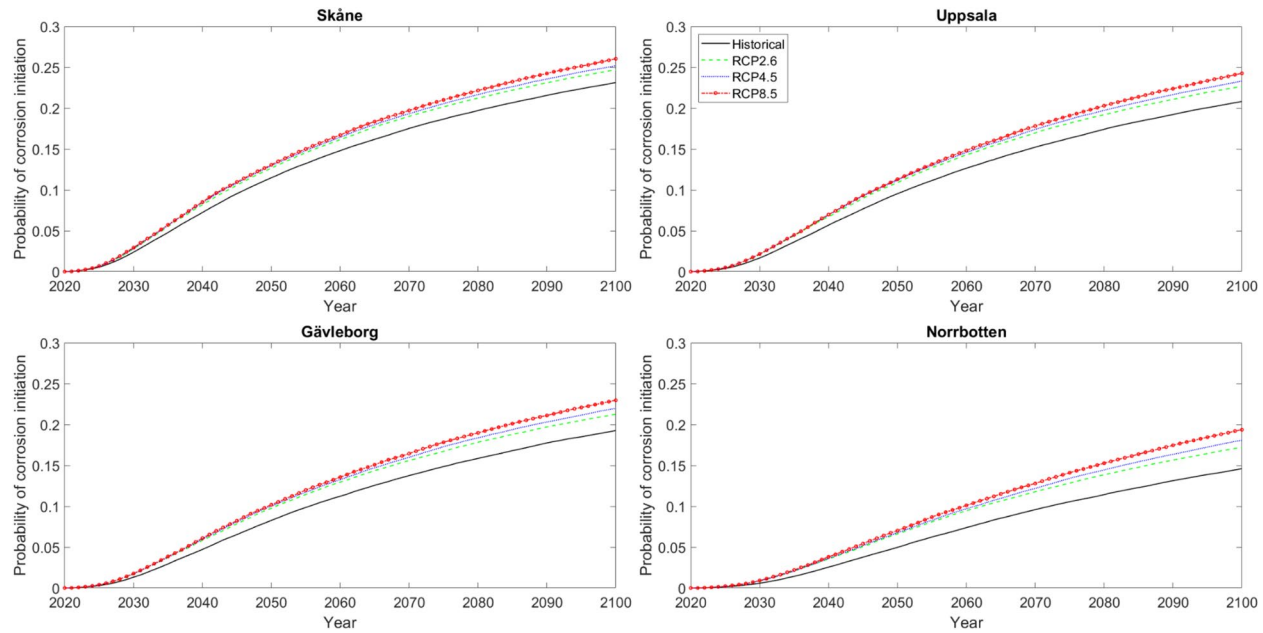

Fig. 5 Probability of corrosion initiation for the studied beam under the historical (1961–1990) and future climatic conditions for Skåne, Uppsala, Gävleborg, and Norrbotten

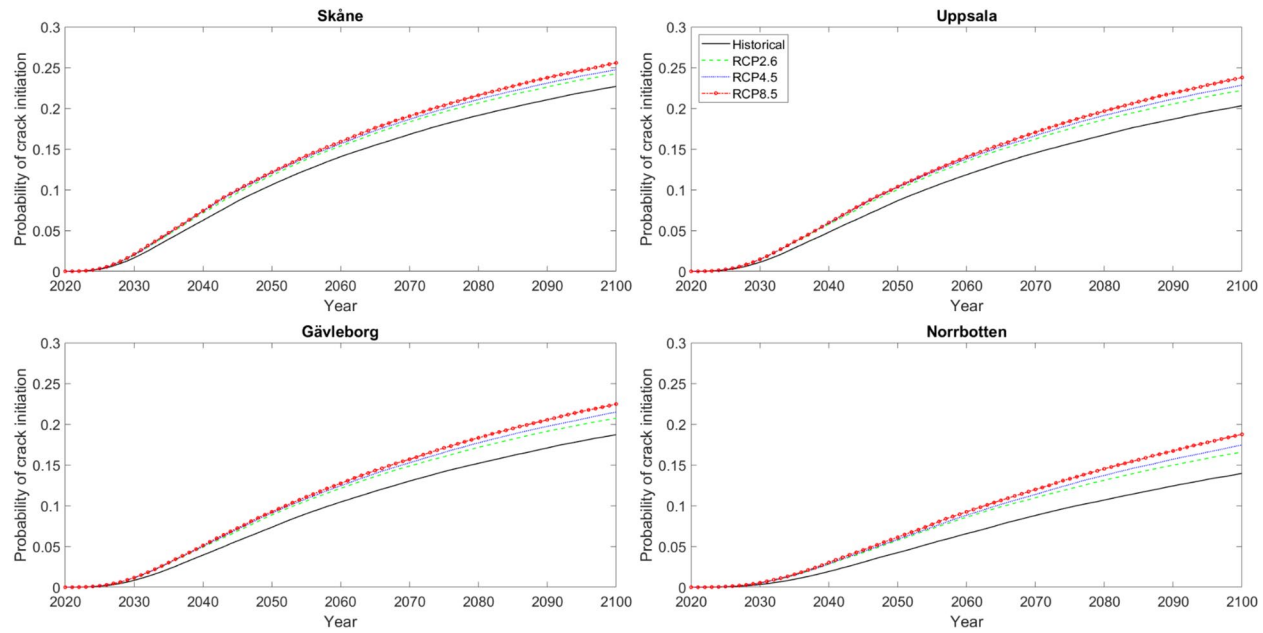

Fig. 6 Probability of crack initiation for the studied beam under the historical (1961–1990) and future climatic conditions for Skåne, Uppsala, Gävleborg, and Norrbotten

of corrosion initiation for all counties in all climate scenarios, the end-of-century probability of severe cracking varies from ~ 0.22 to ~ 0.24 for Skåne, ~ 0.19 to ~ 0.22 for Uppsala, ~ 0.18 to ~ 0.21 for Gävleborg, and ~ 0.13 to ~ 0.17 for Norrbotten depending on the climate scenario.

It is interesting to note that the probability of corrosion initiation (e.g., 0.2605 for Skåne at the end of century in RCP8.5) is very close to the probability of crack initiation (e.g., 0.2558 for Skåne at the end of century in RCP8.5) for all counties in all scenarios. This indicates that the

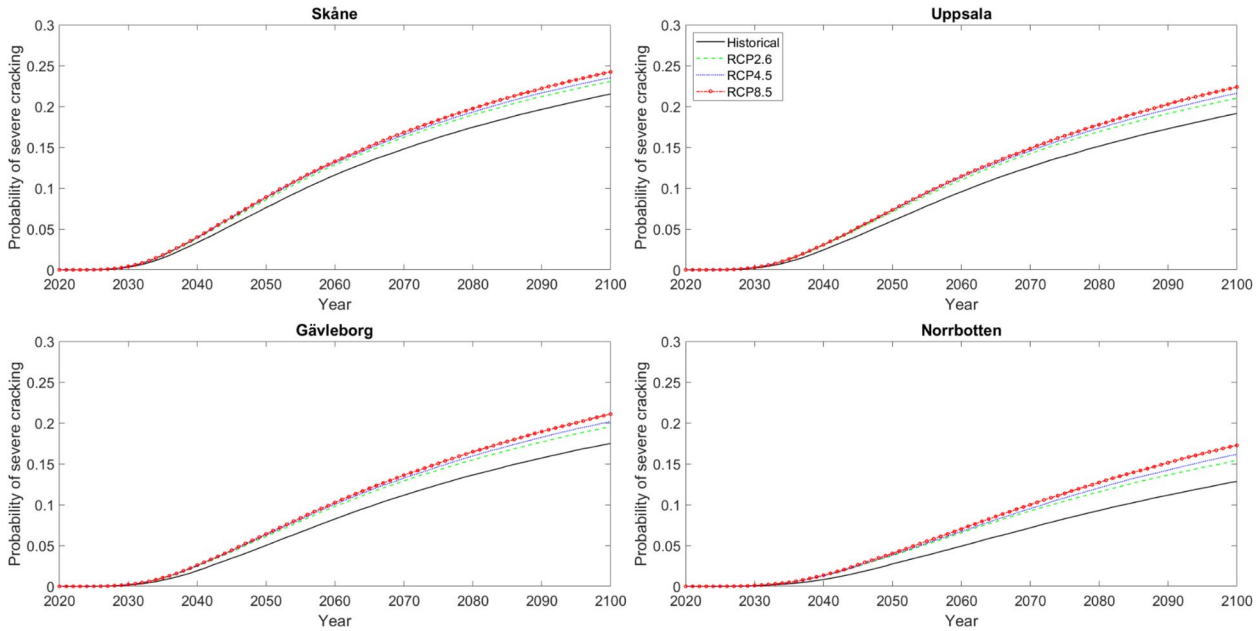

Fig. 7 Probability of severe cracking for the studied beam under the historical (1961–1990) and future climatic conditions for Skåne, Uppsala, Gävleborg, and Norrbotten

time from corrosion initiation until crack initiation is very short compared to the time from the beginning of service life until corrosion initiation. This is in line with previous literature, see, e.g., [6]. Furthermore, the probability of severe cracking (e.g., 0.2424 for Skåne at the end of century in RCP8.5) is also close to the probability of corrosion initiation for all counties in all scenarios. This is also consistent with the findings of other studies, see, e.g., [6].

Table 2 presents the trends of the end-of-century percentage increases in the probabilities of corrosion initiation, crack initiation, and severe cracking due to the different climate change scenarios. It is observed that the percentage increase in these probabilities is highest for Norrbotten followed by Gävleborg, Uppsala, and Skåne, respectively (i.e., an increasing trend from south to north). For Skåne and Uppsala, the end-of-century percentage increase in the probabilities of corrosion initiation, crack initiation, and severe cracking vary from ~ 7% to ~ 13% for Skåne and ~ 9% to ~ 17% for Uppsala (see Table 2). This is generally in line with the observations of Stewart et al. [6] for Sydney and Darwin. For Gävleborg and Norrbotten, on the other hand, the percentage increases in the probabilities of corrosion initiation, crack initiation, and severe cracking can reach up to ~ 20% for Gävleborg and ~ 34% for Norrbotten. Furthermore, Table 2 shows that the percentage increase in the probability of severe cracking is higher than or equal to that in the probability of crack initiation which in turn is higher than or equal to that in the probability of corrosion initiation. For instance, the percentage increases in the probabilities of corrosion initiation, crack initiation, and severe cracking in RCP8.5 for Norrbotten are ~ 33%, ~ 34%, and ~ 34%, respectively.

Time-variant flexural reliability analysis

Figure 8 shows the probability of failure of the studied beam under the historical (1961–1990) and the future climatic conditions in Skåne, Uppsala, Gävleborg, and Norrbotten. From Fig. 8 it can be observed that the probability of failure in all counties is highest in RCP8.5 followed by RCP4.5, RCP2.6, and the historical climate, respectively. It can also be observed that the probability of failure in all climate scenarios is highest in Skåne followed by Uppsala, Gävleborg, and Norrbotten, respectively. These trends are similar to the trends observed for the probabilities of corrosion initiation, crack initiation, and severe cracking in the previous section.

Figure 9 presents the percentage increase in the probability of failure of the studied beam under the three different RCP scenarios for Skåne, Uppsala, Gävleborg, and Norrbotten. The end-of-century percentage increase in the probability of failure is considerably higher (ranging from 3.5–4.9 times higher) than that in the probability of reaching the other limit states. For Norrbotten, for instance, the end-of-century percentage increase in the probability of failure in RCP8.5 is + ~ 123% while the corresponding percentage increase in the probabilities

Table 2 Trends in the end-of-century percentage increases in the probabilities of corrosion initiation, crack initiation, and severe cracking due to climate change for Skåne, Uppsala, Gävleborg, and Norrbotten

Limit state	Scenario	Skåne	Uppsala	Gävleborg	Norrbotten
Corrosion initiation	RCP2.6	+ ~ 7%	+ ~ 9%	+ ~ 10%	+ ~ 18%
	RCP4.5	+ ~ 9%	+ ~ 12%	+ ~ 14%	+ ~ 24%
	RCP8.5	+ ~ 12%	+ ~ 17%	+ ~ 19%	+ ~ 33%
Crack initiation	RCP2.6	+ ~ 7%	+ ~ 9%	+ ~ 11%	+ ~ 19%
	RCP4.5	+ ~ 9%	+ ~ 12%	+ ~ 15%	+ ~ 25%
	RCP8.5	+ ~ 13%	+ ~ 17%	+ ~ 20%	+ ~ 34%
Severe cracking	RCP2.6	+ ~ 7%	+ ~ 10%	+ ~ 12%	+ ~ 20%
	RCP4.5	+ ~ 9%	+ ~ 13%	+ ~ 15%	+ ~ 26%
	RCP8.5	+ ~ 13%	+ ~ 17%	+ ~ 20%	+ ~ 34%

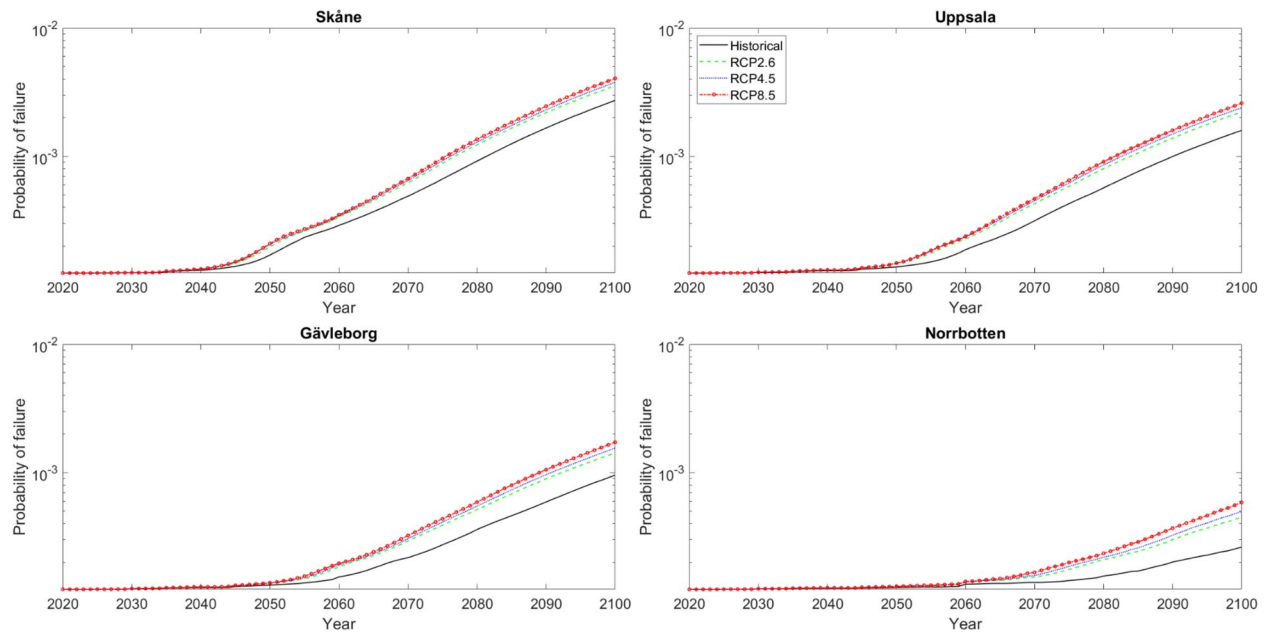

Fig. 8 Probability of failure for the studied beam under the historical (1961–1990) and future climatic conditions for Skåne, Uppsala, Gävleborg, and Norrbotten

of corrosion initiation, crack initiation, and severe cracking are + ~ 32.6%, + ~ 34.3%, and + ~ 34.4%, respectively. Similar to the percentage increases in the probabilities of corrosion initiation, crack initiation, and severe cracking, an increasing trend of the end-of-century percentage increase in the probability of failure can be observed from south to north (i.e., the percentage increase is lowest for Skåne followed by Uppsala, Gävleborg, and Norrbotten). Nonetheless, Fig. 9 reveals that the impact of climate change on the probability of failure depends on the reference period considered. At mid-century, for instance, the aforementioned increasing trend of the percentage increase in the probability of failure from south to north is reversed (i.e., southern counties have higher percentage increases than northern counties).

Sensitivity analysis

To assess the effect of changes in the different parameters involved in the corrosion process and compare this effect to the effect of climate change, a sensitivity analysis is presented herein. Changes to the annual average relative humidity and temperature due to climate change affect the corrosion process by altering the corrosion initiation time and the corrosion rate which subsequently affect the other models presented in Sect. 3. Therefore, the sensitivity analysis in this subsection is limited to the corrosion

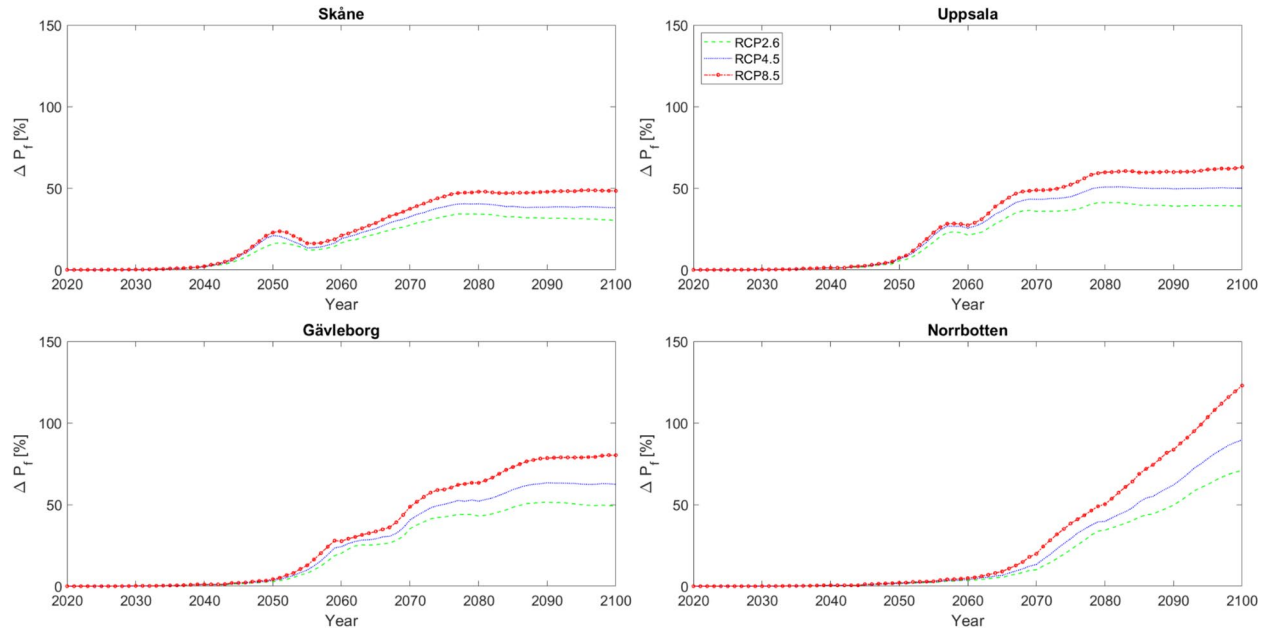

Fig. 9 Percentage change in the probability of failure for the studied beam under the future climatic conditions compared to the historical climate (1961–1990)

initiation and corrosion rate models. The sensitivity analysis is conducted by varying the mean value of each of the input parameters in these two models (one parameter at a time) in the range of -20% – +20% and assessing the change in the output.

Figure 10 presents the percentage change in the end-of-century probability of corrosion initiation considering the historical climate due to changes in the different input parameters in the corrosion initiation model. It can be observed that changes in the parameters C_{cr}, C_s, n_{cl}, and x have the highest effect on the end-of-century probability of corrosion initiation. For instance, a 20% increase in the mean surface chloride concentration (C_s) in Skåne causes ~ 32% increase in the end-of-century probability of corrosion initiation. This effect is close to three times higher than the effect of climate change in the highest emission's scenario (i.e., RCP8.5), see Table 2. The parameters k_e, k_c, k_t, and $D_{c,ref}$ have similar effects ranging from an increase of 11% – 18% and a decrease of -20% – -13% in the probability of corrosion initiation due a 20% increase and decrease, respectively, in their mean values. A 20% increase in the mean value of δ_{t_i} causes a reduction in the range of -14% – -9% while a 20% decrease causes an increase in the range of 12% – 17% in the probability of corrosion initiation. t_0 has only a minor effect of less than 3% increase or reduction in the probability of corrosion initiation for a 20% increase or reduction in its value, respectively.

A reduction in the annual average relative humidity can have a significant effect on the probability of corrosion initiation (a 20% reduction in the mean annual average relative humidity in Skåne causes ~ 35% reduction in the probability of corrosion initiation). On the other hand, a 20% increase in the mean annual average relative humidity causes only a moderate increase in the probability of corrosion initiation (~ 13% in Skåne). Changes in the mean annual average temperature have a smaller effect on the probability of corrosion initiation (limited to ~ 6.6% for a 20% change in the mean annual average temperature). It is important to note, however, that climate change can cause an increase in the mean annual average temperature of up to ~ 145% in the studied counties while its effect on the mean annual relative humidity is limited to less than 3%. The sensitivity of the probability of corrosion initiation to the different input parameters is summarized in Fig. 11. This sensitivity is assessed based on the average absolute slope of the lines in Fig. 10 in the range of -1% – 1% change in the mean value of each parameter.

Figure 12 presents the percentage change in the mean value of the end-of-century corrosion rate considering the historical climate due to changes in the different input parameters in the corrosion initiation and corrosion rate models. It can be observed that changes in the mean values of $\frac{w}{c}$ and the annual average relative humidity have the highest effect on the mean value of

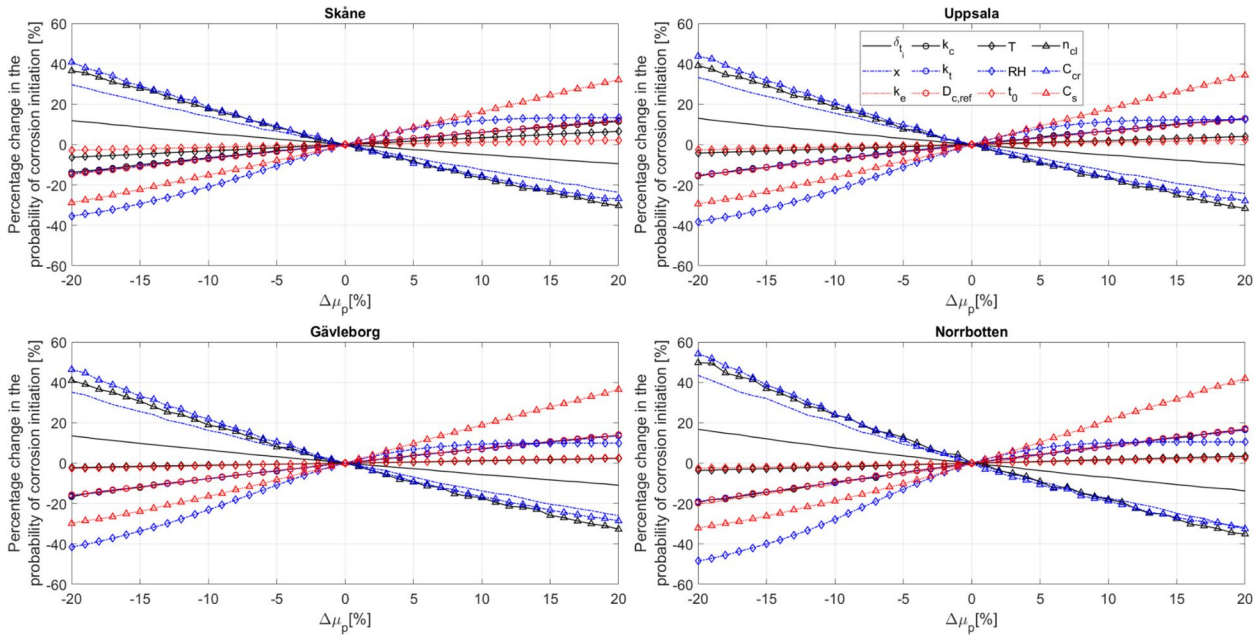

Fig. 10 Percentage change in the end-of-century probability of corrosion initiation due to changes in the mean value of the different input parameters in the corrosion initiation model considering the historical climate (1961–1990)

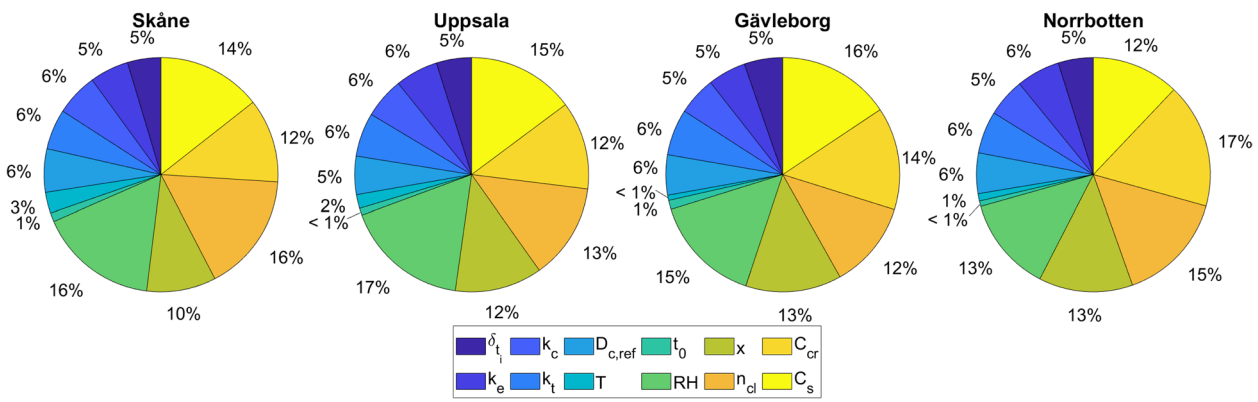

Fig. 11 The sensitivity of the end-of-century probability of corrosion initiation to the different input parameters

the end-of-century corrosion rate. For instance, a 20% increase in the mean value of $\frac{w}{c}$ in Skåne causes ~ 115% increase in the mean value of the end-of-century corrosion rate. It should be noted that, in addition to directly affecting the corrosion rate as seen in Eq. (5), $\frac{w}{c}$ also affects C_s (see the caption of Table 1). Following $\frac{w}{c}$ and the annual average relative humidity, changes in the parameters C_{cr}, C_s, n_{cl}, and x have the next highest effect on the mean value of the corrosion rate. As an example, a 20% increase in the mean surface chloride concentration (C_s) in Skåne causes ~ 47% increase in the mean value of the end-of-century corrosion rate. A 20% increase in the mean value of $\delta_{i_{corr}}$ causes an increase in the vicinity of 20% while a 20% decrease causes a decrease in the vicinity of -20% in the mean value of the end-of-century corrosion rate. A 20% increase and decrease in the mean annual average temperature in Skåne causes changes of + 12% or -11%, respectively, in the mean value of the corrosion rate. Changes in the parameters δ_{t_i}, t_0, k_e, k_c, k_t, and $D_{c,ref}$ have similar effects to those on the probability of corrosion initiation. The sensitivity of the mean value of the end-of-century corrosion rate to the different input parameters is summarized in Fig. 13. This sensitivity is assessed based on the average absolute slope of the lines in Fig. 12 in the range of -1% – 1% change in the mean value of each parameter.

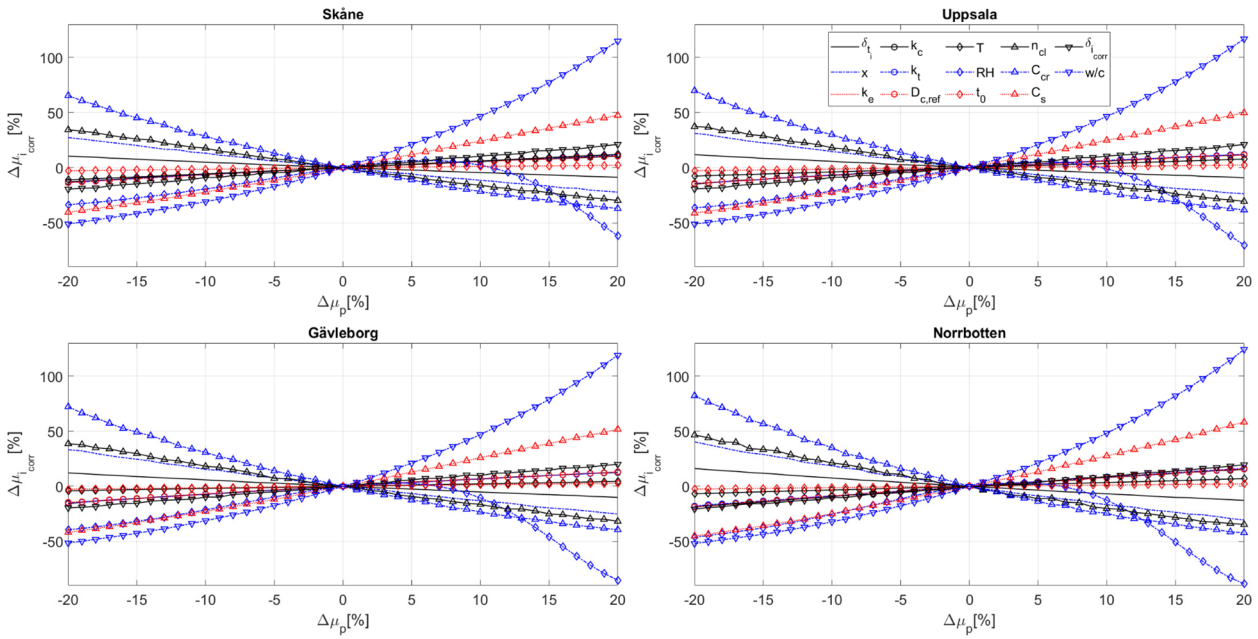

Fig. 12 Percentage change in the mean value of the end-of-century corrosion rate due to changes in the mean value of the different input parameters in the corrosion initiation and corrosion rate models considering the historical climate (1961–1990)

Discussion and conclusions

In the current article, the impact of climate change on chloride-induced corrosion of reinforced concrete structures was studied considering the Swedish climate conditions. It was found that the impact of climate change on the probability of failure can be considerable (reaching up to + ~123% increase by the end of century) especially for northern counties. This impact was found to be considerably higher (ranging from 3.5–4.9 times higher) than the impact of climate change on the probabilities of corrosion initiation, crack initiation, and severe cracking. Furthermore, the impact of climate change at the end of century was found to have an increasing trend from south to north.

An important research gap that was not addressed in the current article (nor in previous studies) concerns the effect of climate change on surface chloride concentrations. Climate change increases ocean salinity in some locations and decreases it in other locations [1]. Hence, the surface chloride concentration (C_s) of marine structures can also be affected by climate change. Noting that the corrosion process is highly sensitive to changes in this parameter (as shown in Sect. 4.3), addressing this research gap is of considerable importance. However, this

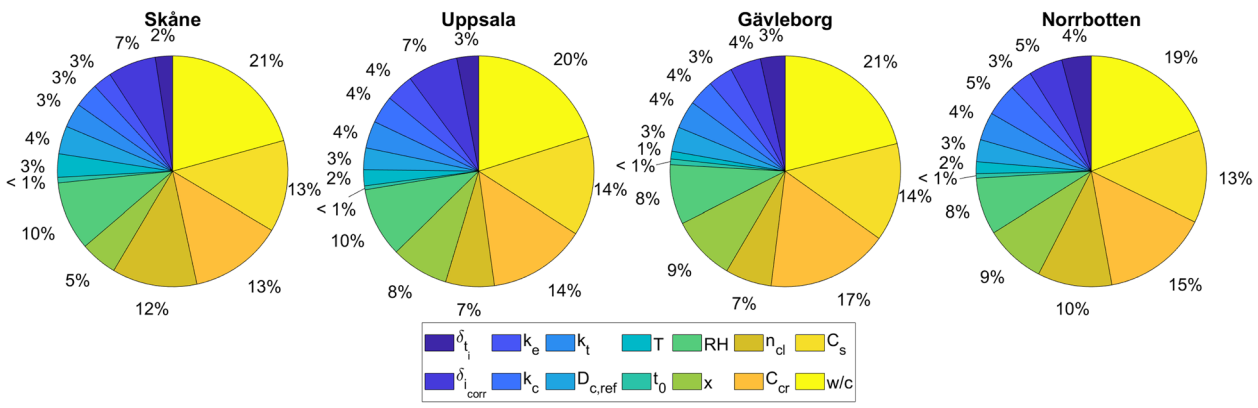

Fig. 13 The sensitivity of the mean value of the end-of-century corrosion rate to the different input parameters

parameter is also dependent on several other local factors such as wind patterns and precipitation (which are both also affected by climate change), distance of structure from ocean, and surface orientation, see, e.g., [67]. The unavailability of the climate data needed hinders the quantification of this effect.

Several other research directions are considered worthwhile. Noting that other studies [6, 25] found that carbonation-induced corrosion of concrete infrastructure is significantly affected by climate change, quantifying this effect for the Swedish climate conditions and its interaction with chloride-induced corrosion is worthy of investigation. Furthermore, a simply supported beam with atmospheric exposure was studied in the current article. The impact of climate change on the corrosion of other reinforced concrete structural elements (e.g., bridge piers) under different exposure conditions (e.g., splash, tidal, or submerged) should be explored. Additionally, the cost-effectiveness of the different adaptation options for the increased impact of infrastructure corrosion [68] (e.g., Using cathodic protection, increasing the concrete cover thickness, or improving the quality of concrete) should be assessed under the Swedish climate conditions. Moreover, future research should address the combined effect of concrete corrosion and other potential climate change impacts on concrete structures (e.g., thermal-stress–strain behaviour [69]). Lastly, assessing the impact of climate change on the reliability of structural elements made of other materials (e.g., timber, steel, and masonry) under Swedish climate conditions is worth exploring.

Acknowledgements
Erik Kjellström and Gustav Strandberg from SMHI are acknowledged for providing the climate model projections.

Authors' contributions
AN conceptualized the study, developed the method, and prepared the original draft of the manuscript. DH and OLI provided critical feedback on the original draft of the manuscript and acquired funding for conducting this study. All authors read and approved the final manuscript.

Funding
Open access funding provided by Lund University. The authors gratefully acknowledge the financial support provided by the Swedish Transport Administration [grant number 2016–008 & 2019–027], the Swedish Research Council (Formas) [grant number 2015–00451], and the strategic innovation program InfraSweden2030 [grant number 2018–00611], a joint effort of Sweden's Innovation Agency (Vinnova), the Swedish Research Council (Formas) and the Swedish Energy Agency (Energimyndigheten). Any opinions, findings, or conclusions stated herein are those of the authors and do not necessarily reflect the opinions of the financiers.

Availability of data and materials
All data that support the findings of this study are available from the corresponding author upon reasonable request (temperature and relative humidity projections).

Declarations

Ethics approval and consent to participate
Not applicable.

Consent for publication
Not applicable.

Competing interests
The authors declare that they have no competing interests.

Author details
[1]Division of Structural Engineering, Lund University, Lund, Sweden. [2]Department of Public Works Engineering, Faculty of Engineering, Mansoura University, Mansoura, Egypt. [3]Transport Department, City of Stockholm, Stockholm, Sweden.

Received: 23 March 2022 Accepted: 28 April 2022
Published online: 21 May 2022

References

1. IPCC (2021) Climate Change 2021: The Physical Science Basis. Contribution of Working Group I to the Sixth Assessment Report of the Intergovernmental Panel on Climate Change. Cambridge University Press, Cambridge
2. Nasr A, Björnsson I, Honfi D, Ivanov O L, Johansson J, Kjellström E (2021) A review of the potential impacts of climate change on the safety and performance of bridges, Sustainable and Resilient Infrastructure, 6:3-4, 192-212. https://doi.org/10.1080/23789689.2019.1593003.
3. Kumar P, Imam B (2013) Footprints of air pollution and changing environment on the sustainability of built infrastructure. Sci Total Environ 444:85–101
4. Meyer M (2008) Design standards for U.S. transportation infrastructure: The implications of climate change. Transportation Research Board, Washington
5. Schwartz HG (2010) Adaptation to the impacts of climate change on transportation. Bridge 40(3):5–13
6. Stewart MG, Wang X, Nguyen MN (2011) Climate change impact and risks of concrete infrastructure deterioration. Eng Struct 33(4):1326–1337
7. Bastidas-Arteaga E, Stewart MG (2015) Damage risks and economic assessment of climate adaptation strategies for design of new concrete structures subject to chloride-induced corrosion. Struct Saf 52:40–53
8. Ryan PC et al (2016) Probabilistic analysis of climate change impacts on timber power pole networks. Int J Electr Power Energy Syst 78:513–523
9. Seo D-W, Caracoglia L (2015) Exploring the impact of "climate change" on lifetime replacement costs for long-span bridges prone to torsional flutter. J Wind Eng Ind Aerodyn 140:1–9
10. Jevrejeva S et al (2018) Flood damage costs under the sea level rise with warming of 15 °C and 2 °C. Environ Res Lett 13(7):1–11
11. Wang X, Stewart MG, Nguyen M (2011) Impact of climate change on corrosion and damage to concrete infrastructure in Australia. Clim Change 110(3–4):941–957
12. Schmitt G (2009) Global needs for knowledge dissemination, research, and development in materials deterioration and corrosion control. World Corrosion Orgnization, New York
13. Nguyen MN, Wang X, Leicester RH (2013) An assessment of climate change effects on atmospheric corrosion rates of steel structures. Corros Eng, Sci Technol 48(5):359–369
14 Koch GH et al (2002) Corrosion cost and preventive strategies in the United States. Federal Highway Administration, United States
15. Kashani MM, Maddocks J, Dizaj EA (2019) Residual Capacity of Corroded Reinforced Concrete Bridge Components: State-of-the-Art Review. J Bridg Eng 24(7):1–16
16 Trafikverket (2020) The Swedish Transport Administration Annual Report 2019. Trafikverket, Borlänge

17. Calvi GM et al (2018) Once upon a Time in Italy: The Tale of the Morandi Bridge. Struct Eng Int 29(2):198–217
18. Malomo D et al (2020) Numerical Study on the Collapse of the Morandi Bridge. J Perform Constr Facil 34(4):1–13
19. Lu X et al (2021) A preliminary analysis and discussion of the condominium building collapse in surfside, Florida, US, June 24, 2021. Front Struct Civ Eng 15(5):1097–1110
20. Jeon D et al (2022) High-accuracy rebar position detection using deep learning–based frequency-difference electrical resistance tomography. Autom Constr 135:1–11
21. Mahmoud H (2020) Barriers to gauging built environment climate vulnerability. Nat Clim Chang 10(6):482–485
22. Biondini F, Frangopol DM (2016) Life-Cycle Performance of Deteriorating Structural Systems under Uncertainty: Review. J Struct Eng 142(9):1–17
23. Monteiro PJM, Miller SA, Horvath A (2017) Towards sustainable concrete. Nat Mater 16(7):698–699
24. Lu Z-H et al (2018) Empirical model of corrosion rate for steel reinforced concrete structures in chloride-laden environments. Adv Struct Eng 22(1):223–239
25. Mortagi M, Ghosh J (2022) Concurrent modelling of carbonation and chloride-induced deterioration and uncertainty treatment in aging bridge fragility assessment, Structure and Infrastructure Engineering. 18:2, 197-218. https://doi.org/10.1080/15732479.2020.1838560.
26. Marquez-Peñaranda JF et al (2015) Effects of biodeterioration on the mechanical properties of concrete. Mater Struct 49(10):4085–4099
27. Bastidas-Arteaga E et al (2008) Coupled reliability model of biodeterioration, chloride ingress and cracking for reinforced concrete structures. Struct Saf 30(2):110–129
28. Zhou Y et al (2015) Carbonation-Induced and Chloride-Induced Corrosion in Reinforced Concrete Structures. J Mater Civ Eng 27(9):1–17
29. Mortagi M, Ghosh J (2020) Climate Change Considerations for Seismic Vulnerability Assessment of Aging Highway Bridges. ASCE-ASME J Risk Uncertainty Eng Syst Part A: Civ Eng 6(1):1–16
30. Bastidas-Arteaga E et al (2010) Influence of weather and global warming in chloride ingress into concrete: A stochastic approach. Struct Saf 32(4):238–249
31. Mortagi M, Ghosh J (2022) Consideration of Climate Change Effects on the Seismic Life-Cycle Cost Analysis of Deteriorating Highway Bridges. J Bridg Eng 27(2):1–18
32. IPCC (2013) Climate Change 2013: The Physical Science Basis- Contribution of Working Group I to the Fifth Assessment Report of the Intergovernmental Panel on Climate Change. Cambridge University Press, Cambridge
33 van Vuuren DP et al (2011) RCP2.6: exploring the possibility to keep global mean temperature increase below 2°C. Climatic Change 109(1–2):95–116
34 Riahi K et al (2011) RCP 8.5—A scenario of comparatively high greenhouse gas emissions. Climatic Change 109(1–2):33–57
35 Thomson AM et al (2011) RCP4.5: a pathway for stabilization of radiative forcing by 2100. Climatic Change 109(1–2):77–94
36. van Vuuren DP et al (2011) The representative concentration pathways: an overview. Clim Change 109(1–2):5–31
37. Kjellström E et al (2016) Production and use of regional climate model projections - A Swedish perspective on building climate services. Clim Serv 2–3:15–29
38. Taylor KE, Stouffer RJ, Meehl GA (2012) An Overview of CMIP5 and the Experiment Design. Bull Am Meteor Soc 93(4):485–498
39. Hazeleger W et al (2010) EC-Earth: A Seamless Earth-System Prediction Approach in Action. Bull Am Meteor Soc 91(10):1357–1364
40. Watanabe S et al (2011) MIROC-ESM 2010: model description and basic results of CMIP5-20c3m experiments. Geoscientific Model Dev 4(4):845–872
41. Collins WJ et al (2011) Development and evaluation of an Earth-System model – HadGEM2. Geoscientific Model Dev 4(4):1051–1075
42. Popke D, Stevens B, Voigt A (2013) Climate and climate change in a radiative-convective equilibrium version of ECHAM6. J Adv Model Earth Syst 5(1):1–14
43. Bentsen M et al (2013) The Norwegian Earth System Model, NorESM1-M – Part 1: Description and basic evaluation of the physical climate. Geoscientific Model Dev 6(3):687–720
44. Val D (2007) Deterioration of strength of RC beams due to corrosion and its influence on beam reliability. J Struct Eng 133:1297–1306
45. Papakonstantinou KG, Shinozuka M (2013) Probabilistic model for steel corrosion in reinforced concrete structures of large dimensions considering crack effects. Eng Struct 57:306–326
46. Jaffer SJ, Hansson CM (2009) Chloride-induced corrosion products of steel in cracked-concrete subjected to different loading conditions. Cem Concr Res 39(2):116–125
47. Enright MP, Frangopol DM (1998) Probabilistic analysis of resistance degredation of reinforced cocncrete bridge beams under corrosion. Eng Struct 20(11):960–971
48. Duracrete (2000) Probabilistic performance based durability design of concrete structures. European Union, Brussels
49. Val D, Trapper P (2008) Probabilistic evaluation of initiation time of chloride-induced corrosion. Reliab Eng Syst Saf 93:364–372
50. Choe D-E et al (2008) Probabilistic capacity models and seismic fragility estimates for RC columns subject to corrosion. Reliab Eng Syst Saf 93(3):383–393
51. Choe D-E et al (2009) Seismic fragility estimates for reinforced concrete bridges subject to corrosion. Struct Saf 31(4):275–283
52. Vu KA, Stewart MG (2000) Structural reliability of concrete bridges including improved chloride-induced corrosion models. Struct Saf 22:313–333
53. Guo Y, Trejo D, Yim S (2015) New Model for Estimating the Time-Variant Seismic Performance of Corroding RC Bridge Columns. J Struct Eng 141(6):1–12
54. Chernin L, Val DV (2011) Prediction of corrosion-induced cover cracking in reinforced concrete structures. Constr Build Mater 25(4):1854–1869
55. Rodriguez J, Ortega L M, Casal J, Diez J M (1996) Corrosion of reinforcement and service life of concrete structures, Durab Build Mater Compon. 7:1, 117–126.
56. Vu KA, Stewart MG, Mullard J (2005) Corrosion-induced cracking: Experimental data and predictive models. ACI Struct J 102(5):719–726
57. Mullard JA, Stewart MG (2011) Corrosion-induced cover cracking: new test data and predictive models. ACI Struct J 108(1):71–79
58. Ghosh J, Sood P (2016) Consideration of time-evolving capacity distributions and improved degradation models for seismic fragility assessment of aging highway bridges. Reliab Eng Syst Saf 154:197–218
59. Val D, Melchers RE (1997) Reliability of deteriorating RC slab bridges. J Struct Eng 123(12):1638–1644
60. Stewart MG (2004) Spatial variability of pitting corrosion and its influence on structural fragility and reliability of RC beams in flexure. Struct Saf 26(4):453–470
61. Kim J, Song J (2021) Time-Dependent Reliability Assessment and Updating of Post-tensioned Concrete Box Girder Bridges Considering Traffic Environment and Corrosion. ASCE-ASME J Risk Uncertainty Eng Syst Part A Civil Eng 7(4):1–18
62. Cairns J et al (2005) Mechanical properties of corrosion-damaged reinforcement. ACI Mater J 102(4):256–264
63. Du YG, Clark LA, Chan AHC (2005) Effect of corrosion on ductility of reinforcing bars. Mag Concr Res 57(7):407–419
64. Feng D-C et al (2021) Time-dependent reliability-based redundancy assessment of deteriorated RC structures against progressive collapse considering corrosion effect. Struct Saf 89:1–17
65. BenSeghier MEA, Keshtegar B, Mahmoud H (2021) Time-Dependent Reliability Analysis of Reinforced Concrete Beams Subjected to Uniform and Pitting Corrosion and Brittle Fracture. Materials (Basel) 14(8):1–15
66. Hamidane H et al (2020) Reliability analysis of corrosion initiation in reinforced concrete structures subjected to chlorides in presence of epistemic uncertainties. Struct Saf 86:1–12
67. Borah MM, Dey A, Sil A (2020) Service life assessment of chloride affected bridge located in coastal region of India considering variation in the inherent structural parameters. Structures 23:191–203
68. Nasr A et al (2020) Bridges in a changing climate: a study of the potential impacts of climate change on bridges and their possible adaptations. Struct Infrastruct Eng 16(4):738–749
69. Santillán D, Salete E, Toledo MÁ (2015) A methodology for the assessment of the effect of climate change on the thermal-strain–stress behaviour of structures. Eng Struct 92:123–141

Publisher's Note